Selective para-Halogenation and Dimerization of N,C,N '-Arylruthenium(II) and -(III) 2,2:6 ',2 ''-Terpyridine Cations

ARTICLE *in* JOURNAL OF THE AMERICAN CHEMICAL SOCIETY · FEBRUARY 2010

Impact Factor: 12.11 · DOI: 10.1021/ja9073276 · Source: PubMed

6 AUTHORS, INCLUDING:

Anthony L. Spek
Utrecht University
1,591 PUBLICATIONS **55,075** CITATIONS
SEE PROFILE

Gerard van koten
Utrecht University
1,113 PUBLICATIONS **28,237** CITATIONS
SEE PROFILE

J|A|C|S ARTICLES

Published on Web 01/20/2010

Selective *para*-Halogenation and Dimerization of *N,C,N′*-Arylruthenium(II) and -(III) 2,2′:6′,2″-Terpyridine Cations

Sipke H. Wadman,[†] Remco W. A. Havenith,[‡] Martin Lutz,[§] Anthony L. Spek,[§] Gerard P. M. van Klink,[†,||] and Gerard van Koten*[,†]

Chemical Biology & Organic Chemistry and Theoretical Chemistry, Debije Institute for Nanomaterials Science, and Crystal & Structural Chemistry, Bijvoet Center for Biomolecular Research, Faculty of Science, Utrecht University, Padualaan 8, 3584 CH Utrecht, The Netherlands

Received September 20, 2009; E-mail: g.vankoten@uu.nl

Abstract: The *N,C,N′*-bonded arylruthenium 2,2′:6′,2″-terpyridine (tpy) complex salts [Ru(NCN)(tpy)](Cl) ([**1a**](Cl), NCN = 2,6-bis[(dimethylamino)methyl]phenyl) and [Ru(N^C^N)(tpy)](PF_6), ([**2a**](PF_6), N^C^N = 2,6-bis(2-pyridyl)phenyl) can be halogenated under very mild conditions by oxidation with copper(II) halogen salts. Halogenation occurs exclusively *para* to the site of metalation and yields the cations [Ru(4-R-NCN)(tpy)]$^+$ (*R* = Cl, [**1b**]$^+$ and *R* = Br [**1c**]$^+$) and [Ru(4-R-N^C^N)(tpy)]$^+$ (R = Cl, [**2b**]$^+$ and R = Br [**2c**]$^+$). In the presence of an excess of oxidant relative to [**1a**]$^+$, the halogenation reaction follows first order kinetics in the oxidized ruthenium complex. However, by using a small excess of copper(II) compared to [**1a**]$^+$, dimerization of the complex cation to [{Ru(tpy)}$_2$(μ-NCN-NCN)]$^{4+}$ ([**3**]$^{4+}$) is observed, which obeys second order kinetics. Both halogenation (C−X coupling) and dimerization (C−C coupling) are a result of the unique properties of the ruthenium(III) complexes compared to their parent ruthenium(II) species. According to the nature of the highest occupied spin orbital (HOSO) in DFT calculations the unpaired electron in [**1a**]$^{2+}$ and [**2a**]$^{2+}$ is partially localized on the *para* position. The involvement of the cyclometalated ligand in the HOSO is supported by redox data and electronic absorption spectroscopy. The ruthenium(III) species can best be considered a persistent organometallic radical.

Introduction

Performing reactions on (organometallic) complexes still is a challenging field of research.[1−6] *Post*-coordination functionalization offers the possibility to introduce substituents that are orthogonal to the conditions used to form the complex.[1,2,7,8] Specifically, the presence of peripheral halogen substituents are problematic when complex formation involves lithiation of the ligand. Particularly interesting in this aspect are cyclometalated complexes, in which a covalent carbon-to-metal bond is part of a polydentate bonded ligand.[1,9−12] One of the features of cyclometalation is that the electron density in the *C*-metalated ring is increased at the positions *para* and *meta* to the site of C-metalation. This favors electrophilic reactions such as bromination or nitration to occur at conditions that are mild in comparison to the conditions needed for the uncoordinated systems.[13−15] For instance, bromination of organometallic complexes of ruthenium as well as other metals have been performed using NBS,[15,16] pyridinium tribromide,[13,17,18] or

[†] Chemical Biology & Organic Chemistry, Utrecht University.
[‡] Theoretical Chemistry Group, Utrecht University, also associated with Electronic Structure of Materials, Radboud University Nijmegen, Heyendaalseweg 135, 6525 AJ Nijmegen, The Netherlands.
[§] Crystal & Structural Chemistry, Utrecht University.
[||] Present address; DelftChemTech, Faculty of Applied Sciences, Delft University of Technology, Julianalaan 136, 2628 BL Delft, The Netherlands.

(1) Gagliardo, M.; Snelders, D. J. M.; Chase, P. A.; Klein Gebbink, R. J. M.; van Klink, G. P. M.; van Koten, G. *Angew. Chem., Int. Ed.* **2007**, *46* (45), 8558–8573.
(2) Harre, K.; Enkelmann, V.; Schulze, M.; Bunz, U. H. F. *Chem. Ber.* **1996**, *129* (11), 1323–1325.
(3) Fraysse, S.; Coudret, C.; Launay, J.-P. *J. Am. Chem. Soc.* **2003**, *125* (19), 5880–5888.
(4) Aspley, C. J.; Williams, J. A. G. *New. J. Chem.* **2001**, *25* (9), 1136–1147.
(5) Arm, K. J.; Williams, J. A. G. *Dalton Trans.* **2006**, (18), 2172–2174.
(6) Griffiths, P. M.; Loiseau, F.; Puntoriero, F.; Serroni, S.; Campagna, S. *Chem. Commun.* **2000**, (23), 2297–2298.
(7) Gagliardo, M.; Rodriguez, G.; Dam, H. H.; Lutz, M.; Spek, A. L.; Havenith, R. W. A.; Coppo, P.; De Cola, L.; Hartl, F.; van Klink, G. P. M.; van Koten, G. *Inorg. Chem.* **2006**, *45* (5), 2143–2155.
(8) Vrabel, M.; Pohl, R.; Klepetarova, B.; Votruba, I.; Hocek, M. *Org. Biomol. Chem.* **2007**, *5* (17), 2849–2857.
(9) Barigelletti, F.; Ventura, B.; Collin, J. P.; Kayhanian, R.; Gavina, P.; Sauvage, J. P. *Eur. J. Inorg. Chem.* **2000**, (1), 113–119.
(10) Albrecht, M.; van Koten, G. *Angew. Chem., Int. Ed.* **2001**, *40* (20), 3750–3781.
(11) Collin, J. P.; Gavina, P.; Heitz, V.; Sauvage, J. P. *Eur. J. Inorg. Chem.* **1998**, (1), 1–14.
(12) Kui, S. C. F.; Sham, I. H. T.; Cheung, C. C. C.; Ma, C. W.; Yan, B. P.; Zhu, N. Y.; Che, C. M.; Fu, W. F. *Chem.—Eur. J.* **2007**, *13* (2), 417–435.
(13) Clark, A. M.; Rickard, C. E. F.; Roper, W. R.; Wright, L. J. *Organometallics* **1999**, *18* (15), 2813–2820.
(14) Clark, G. R.; Headford, C. E. L.; Roper, W. R.; Wright, L. J.; Yap, V. P. D. *Inorg. Chim. Acta* **1994**, *220* (1−2), 261–272.
(15) Coudret, C.; Fraysse, S.; Launay, J. P. *Chem. Commun.* **1998**, (6), 663–664.
(16) Arm, K. J.; Williams, J. A. G. *Chem. Commun.* **2005**, (2), 230–232.
(17) Cheung, K.-M.; Zhang, Q.-F.; Chan, K.-W.; Lam, M. H. W.; Williams, I. D.; Leung, W.-H. *J. Organomet. Chem.* **2005**, *690* (12), 2913–2921.
(18) Clark, A. M.; Rickard, C. E. F.; Roper, W. R.; Wright, L. J. *J. Organomet. Chem.* **2000**, *598* (2), j262–275.

 10.1021/ja9073276

Chart 1. Molecular Structures and NMR Numbering Scheme for Ruthenium(II) Cations $[Ru(NCN)(tpy)]^+$, $[\mathbf{1}]^+$, and $[Ru(N\hat{}C\hat{}N)(tpy)]^+$, $[\mathbf{2}]^+$

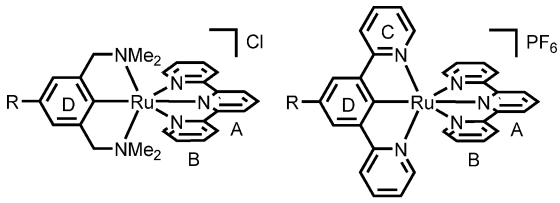

R = H $[\mathbf{1a}]^+$ R = Cl $[\mathbf{1b}]^+$ R = Br $[\mathbf{1c}]^+$

R = H $[\mathbf{2a}]^+$ R = Cl $[\mathbf{2b}]^+$ R = Br $[\mathbf{2c}]^+$

bromine[19] at ambient conditions. Additionally, the oxidation sensitive donor heteroatoms are protected by coordination to the metal center. Oxidation of a cyclometalated complex changes the electron density distribution in the complex significantly, and often severely altered chemistry is observed. For instance, the one-electron oxidized ruthenium(III) complex [Ru(NCN)(tpy)]$^{2+}$ ($[\mathbf{1a}]^{2+}$, NCN-pincer = 2,6-bis[(dimethylamino)methyl]phenyl, tpy = 2,2′:6′,2″-terpyridine) forms the C−C coupled dimer in solution, while such behavior is not observed for the ruthenium(II) complex.[20−22]

Herein, we describe a new methodology of performing halogenations on *N*,*C*,*N*′-cyclometalated arylruthenium tpy cationic complexes by utilizing the unique properties of the corresponding oxidized ruthenium precursors. Using the complexes $[Ru(NCN)(tpy)]^+$ ($[\mathbf{1a}]^+$) with amino nitrogen donor atoms and $[Ru(N\hat{}C\hat{}N)(tpy)]^+$ ($[\mathbf{2a}]^+$, N^C^N = 1,3-bis(2-pyridyl)benzene) with pyridyl nitrogen donor atoms we investigate the effect of the metalated ligands on the reactivity of the corresponding ruthenium complexes. It was found that selective halogenation can be performed even on complex $[\mathbf{1a}]^{2+}$, for which the usually applied mild conditions are too harsh. Additionally, we investigate the electronic and photophysical properties of these *N*,*C*,*N*′-cyclometalated ruthenium(II) and ruthenium(III) cationic complexes. Density functional theory (DFT) and time-dependent DFT (TD-DFT) calculations have been applied to rationalize the reactivity of the complexes and to correlate this to experimental analytical data.

Results

Synthesis. Complexes $[\mathbf{1a}](Cl)$[23] and $[\mathbf{2a}](PF_6)$,[24] Chart 1, were prepared according to previously published procedures and their NMR spectra are in concert with those reported. Complexes $[\mathbf{1}]^+$ were consistently isolated as the corresponding chloride salt while the hexafluorophosphate anion was employed for the complexes $[\mathbf{2}]^+$. As a number of different, potential counter-anions were present in the reaction mixture the purity of the isolated complexes was ensured by subsequent anion exchange.

Halogenation in the *para*-position of the cyclometalated aryl was performed by reaction of either $[\mathbf{1a}]^+$ or $[\mathbf{2a}]^+$ with an excess of CuX_2 salt, Scheme 1. Upon addition of an intensely blue colored solution of $[\mathbf{1a}](Cl)$ to a turquoise MeOH solution of excess $CuCl_2$ (42 equivalents) the characteristic blue color of $[\mathbf{1a}]^+$ disappeared immediately, and the resulting solution was colored red. The optical density in the visible region of the copper(II) (and copper(I)) species in the solution was low compared to that of the ruthenium species and the observed color change was thus primarily associated with the *in situ* oxidation of $[\mathbf{1a}]^+$ to $[\mathbf{1a}]^{2+}$. After stirring overnight, the ruthenium(III) complex $[\mathbf{1b}]^{2+}$ was formed. After reduction of $[\mathbf{1b}]^{2+}$ with $Na_2S_2O_3$ the ruthenium(II) complex $[\mathbf{1b}](Cl)$ was isolated. Similarly, $[\mathbf{1c}]^+$ was prepared from $[\mathbf{1a}]^+$ by reaction with $CuBr_2$ (22 equiv). To prevent halogen scrambling due to the chloride counteranion, $[\mathbf{1a}](Cl)$ was converted to the bromide salt $[\mathbf{1a}](Br)$ prior to reaction.

The dimeric complex $[\{Ru(tpy)\}_2(\mu\text{-NCN-NCN})](CuCl_2)_4$ ($[\mathbf{3}]^{4+}$) was available from previous studies in which it was prepared by dimerization, via C−C coupling, of $[\mathbf{1a}]^+$ in methanol solution after oxidation to $[\mathbf{1a}]^{2+}$ with a small excess (3 equivalents) of $CuCl_2$.[20,22] Sauvage et al. showed that the dimer $[\{Ru(ttpy)\}_2(\mu\text{-N}\hat{}C\hat{}N\text{−N}\hat{}C\hat{}N)]^{2+}$ was obtained in a similar fashion after oxidation of $[Ru(N\hat{}C\hat{}N)(ttpy)]^+$ (ttpy = 4′-tolyl-2,2′:6′,2″-terpyridine) by $AgBF_4$.[25,26]

The ^1H and ^{13}C NMR spectra and MALDI-TOF mass spectra of the ruthenium(II) complexes $[\mathbf{1b}]^+$ and $[\mathbf{1c}]^+$ were consistent with selective introduction of the halogen *para* to the cyclometalated carbon. In particular the ^1H NMR resonance of the proton coded D4 had disappeared and the proton coded D3 was observed as a singlet.

Whereas the paramagnetic ruthenium(III) complex $[\mathbf{1a}]^{2+}$ is reactive and could only be isolated by precipitation from water,[20,21] the complexes $[\mathbf{1b}]^{2+}$ and $[\mathbf{1c}]^{2+}$ could be isolated as the PF_6 salts prior to their reduction to the corresponding ruthenium(II) cations and were also analyzed using ^1H NMR spectroscopy in CD_3CN solution, Figure 1. Large paramagnetic shifts were observed as a result of the unpaired electron. Unfortunately, fast relaxation did not allow assignment of the spectra using two-dimensional spectroscopic techniques. However, eight of the expected nine signals for $[\mathbf{1b}]^{2+}$ and $[\mathbf{1c}]^{2+}$ were resolved indeed, and the resonances for the NMe_2 groups were probably represented by the broad bump ranging from −10 to 40 ppm as a result of paramagnetic broadening. Additionally, the molecular structure of $[\mathbf{1b}](PF_6)_2$ was confirmed by single crystal X-ray structure determination, *vide infra*. In spite of the fact that the ruthenium(II) complexes $[\mathbf{1}]^+$ and the ruthenium(III) complexes $[\mathbf{1}]^{2+}$ are indefinitely stable as a solid, they slowly photodecomposed in solution over the course of several days.

Halogenation of $[\mathbf{2a}](PF_6)$ was attempted in a similar fashion as applied for $[\mathbf{1a}](Cl)$. However, the characteristic red color of $[\mathbf{2a}]^+$ was preserved upon addition of $[\mathbf{2a}]^+$ to excess (21 equiv) of $CuCl_2$ in MeOH solution. Complete conversion of $[\mathbf{2a}]^+$ to $[\mathbf{2b}]^+$ was only observed after heating the solution under reflux for 72 h. On the other hand, addition of a red solution of $[\mathbf{2a}]^+$ to a brownish MeOH solution of $CuBr_2$ (18 equiv) results in an immediate color change to bright green associated with

(19) Ghosh, R.; Emge, T. J.; Krogh-Jespersen, K.; Goldman, A. S. *J. Am. Chem. Soc.* **2008**, *130* (34), 11317–11327.
(20) Sutter, J. P.; Grove, D. M.; Beley, M.; Collin, J. P.; Veldman, N.; Spek, A. L.; Sauvage, J. P.; van Koten, G. *Angew. Chem., Int. Ed.* **1994**, *33* (12), 1282–1285.
(21) Steenwinkel, P.; Grove, D. M.; Veldman, N.; Spek, A. L.; van Koten, G. *Organometallics* **1998**, *17* (26), 5647–5655.
(22) Gagliardo, M.; Amijs, C. H. M.; Lutz, M.; Spek, A. L.; Havenith, R. W. A.; Hartl, F.; van Klink, G. P. M.; van Koten, G. *Inorg. Chem.* **2007**, *46* (26), 11133–11144.
(23) Sutter, J. P.; James, S. L.; Steenwinkel, P.; Karlen, T.; Grove, D. M.; Veldman, N.; Smeets, W. J. J.; Spek, A. L.; van Koten, G. *Organometallics* **1996**, *15* (3), 941–948.
(24) Wadman, S. H.; Lutz, M.; Tooke, D. M.; Spek, A. L.; František, H.; Havenith, R. W. A.; van Klink, G. P. M.; van Koten, G. *Inorg. Chem.* **2009**, *48* (5), 1887–1900.
(25) Beley, M.; Collin, J. P.; Sauvage, J. P. *Inorg. Chem.* **1993**, *32* (21), 4539–4543.
(26) Beley, M.; Collin, J. P.; Louis, R.; Metz, B.; Sauvage, J. P. *J. Am. Chem. Soc.* **1991**, *113* (22), 8521–8522.

Scheme 1. Chlorination of $[\mathbf{1a}]^+$ by $CuCl_2$

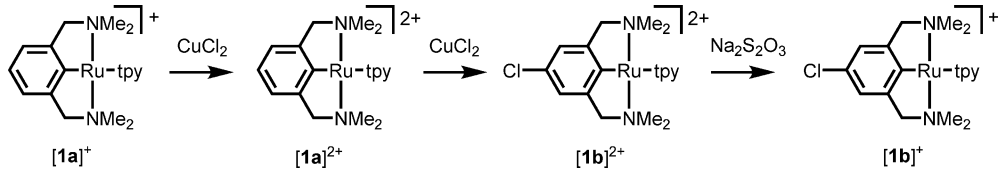

the ruthenium(III) complex $[\mathbf{2a}]^{2+}$. After overnight stirring at room temperature, $[\mathbf{2c}]^+$ was isolated after reduction with $Na_2S_2O_3$. Selective introduction of the bromine substituent in *para*-position was confirmed by ^1H and ^{13}C NMR spectroscopy and MALDI-TOF mass spectroscopy. Complexes $[\mathbf{2}]^+$ and $[\mathbf{2}]^{2+}$ are stable both as solid and in solution. In the course of several weeks, a MeCN solution of bright green $[\mathbf{2a}]^{2+}$ was partially photoreduced by ambient light to red $[\mathbf{2a}]^+$.

Molecular Structure of [Ru(NCN)(tpy)](PF$_6$)$_2$, [1b](PF$_6$)$_2$. Single crystals of ruthenium(III) complex $[\mathbf{1b}](PF_6)_2$, suitable for X-ray crystal structure determination could be obtained by slow evaporation of a MeCN solution. The molecular structure of cation $[\mathbf{1b}]^{2+}$ is depicted in Figure 2. Selected bond lengths and angles for the three independent molecules of $[\mathbf{1b}]^{2+}$ are given in Table 1. Corresponding parameters for the previously reported molecular structure of ruthenium(II) complex [**1a**](Cl) are included for comparison.[23]

The ruthenium(III) ion has a smaller ionic radius as well as a higher charge than the ruthenium(II) ion, which is reflected in the molecular structure. Most notable difference between the ruthenium(II) and ruthenium(III) species is the shortening of the C_{ipso}-to-ruthenium bond lengths of 1.983(8) Å in $[\mathbf{1a}]^+$ to 1.945(2)−1.954(3) in $[\mathbf{1b}]^{2+}$. This shorter bond results in a better fit of the NCN-pincer ligand to the octahedral coordination

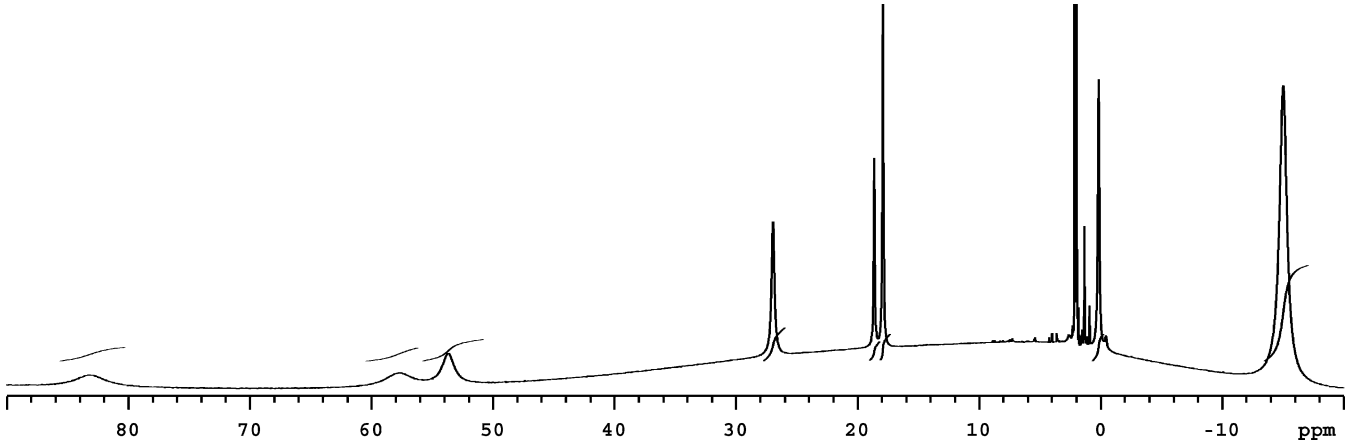

Figure 1. ^1H NMR spectrum of $[\mathbf{1b}]^{2+}$.

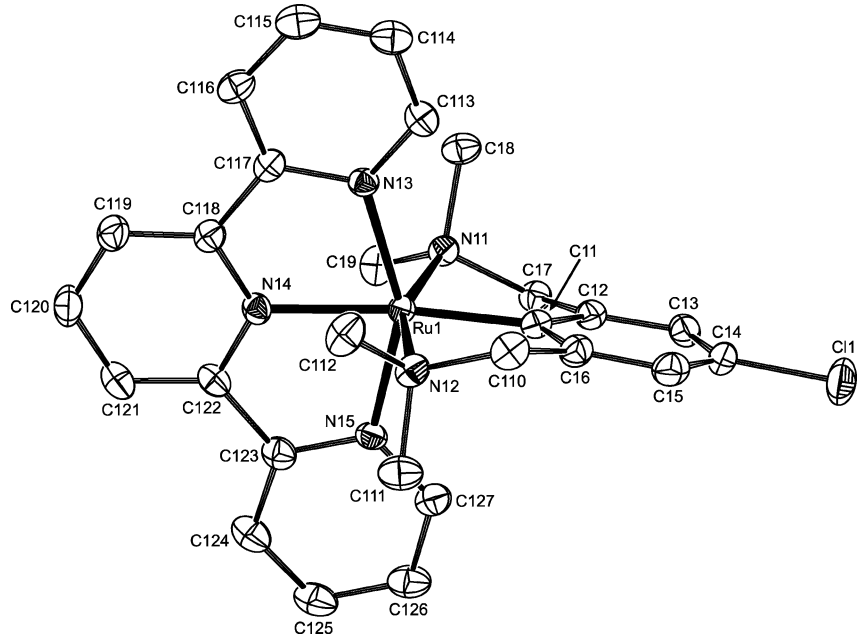

Figure 2. Displacement ellipsoid plot (50% probability level) of the Ru(III) cation $[\mathbf{1b}]^{2+}$. Only one of three independent molecules is shown. Hydrogen atoms, PF_6^- counter-anions, and MeCN solvent molecules have been omitted for clarity.

Table 1. Selected Bond Lengths (Å) and Angles (deg) for the Three Independent Molecules of $[\mathbf{1b}]^{2+}$ and the Corresponding Values for $[\mathbf{1a}]^{+}$[23]

	$[\mathbf{1b}]^{2+}$			
	$x = 1$	$x = 2$	$x = 3$	$[\mathbf{1a}]^{+}$
Ru(x)−C(x1)	1.954(3)	1.945(2)	1.949(3)	1.983(8)
Ru(x)−N(x1)	2.193(2)	2.189(2)	2.184(2)	2.199(7)
Ru(x)−N(x2)	2.206(2)	2.199(2)	2.199(2)	2.192(7)
Ru(x)−N(x3)	2.088(2)	2.089(2)	2.089(2)	2.077(6)
Ru(x)−N(x4)	2.097(2)	2.092(2)	2.092(2)	2.007(6)
Ru(x)−N(x5)	2.107(2)	2.109(2)	2.111(2)	2.087(6)
C(x1)−C(x2)	1.406(4)	1.403(4)	1.400(4)	1.398(11)
C(x2)−C(x3)	1.373(4)	1.391(4)	1.378(4)	1.379(11)
C(x3)−C(x4)	1.398(4)	1.391(4)	1.398(4)	1.380(13)
C(x4)−C(x5)	1.386(4)	1.408(4)	1.377(4)	1.386(13)
C(x5)−C(x6)	1.388(4)	1.374(4)	1.380(4)	1.395(11)
C(x6)−C(x1)	1.405(4)	1.407(4)	1.417(4)	1.412(11)
C(x4)−Cl(x)	1.746(3)	1.740(3)	1.752(3)	
N(x1)−Ru(x)−N(x2)	160.06(8)	160.77(8)	160.75(8)	156.2(3)
N(x3)−Ru(x)−N(x5)	152.54(8)	152.55(8)	152.56(9)	156.9(3)
C(x1)−Ru(x)−N(x4)	173.90(10)	172.74(10)	171.93(9)	178.4(4)

Table 2. Cyclic Voltammetric Data for $[\mathbf{1}]^{+}$,[a] $[\mathbf{2}]^{+}$,[b] and $[Ru(tpy)_2]^{2+}$

	$E_{1/2}$ (V) (ΔE_p (mV))		
complex	second oxidation	Ru^{II}/Ru^{III}	tpy/tpy$^{\bullet-}$
$[\mathbf{1a}]^{+}$	0.66[c]	−0.18 (61)	−2.03(63)
$[\mathbf{1b}]^{+}$	0.68[c]	−0.10(65)	−2.00(66)
$[\mathbf{1c}]^{+}$	0.63[c]	−0.12(64)	−2.01(66)
$[\mathbf{3}]^{2+}$[d]	−0.25	−0.07	−1.97
$[\mathbf{2a}]^{+}$	1.26[c]	0.12 (62)	−1.95(63)
$[\mathbf{2b}]^{+}$	1.29[c]	0.17(64)	−1.93(69)
$[\mathbf{2c}]^{+}$	1.32[c]	0.16(65)	−1.93(71)
$[Ru(tpy)_2]^{2+}$		0.89	−1.66

[a] Data collected in MeCN with $[n\text{-}Bu_4N]PF_6$ as supporting electrolyte at 100 mV/s; potentials reported relative vs ferrocene/ferrocenium (Fc/Fc^{+}) used as external standard. [b] Versus Fc/Fc^{+} used as internal reference. [c] Irreversible, $E_{p,a}$ reported. [d] In PrCN solution.[20−22]

geometry of the ruthenium ion in $[\mathbf{1b}]^{2+}$. The N11−Ru1−N12 angle of 160.06(8)−160.77(8)° in $[\mathbf{1b}]^{2+}$ is closer to the ideal value of 180° compared to 156.2(3)° in $[\mathbf{1a}]^{+}$. On the other hand, the central tpy nitrogen-to-ruthenium bond is lengthened in $[\mathbf{1b}]^{2+}$ by almost 0.1 Å, decreasing the N13−Ru1−N15 angle from 156.9(3) in $[\mathbf{1a}]^{+}$ to 152.54(8)−152.56(8) in $[\mathbf{1b}]^{2+}$, reflecting the increased *trans*-influence of the C_{ipso}-to-ruthenium bond.

Electrochemical Data. Complexes $[\mathbf{1}]^{+}$ and $[\mathbf{2}]^{+}$ show rich redox chemistry in MeCN solution, Table 2. The noncyclometalated ruthenium(II) complex $[Ru(tpy)_2]^{2+}$ was available from previous studies and its oxidation ($E_{1/2} = 0.89$ V) and reduction ($E_{1/2} = -1.66$ V) potentials in the present study are in concert with the reported values of 0.92 and −1.67 V, respectively, also obtained in MeCN solution.[27] Polypyridine complexes of ruthenium(II) are characterized by a metal-based initial anodic process and ligand-based first cathodic process.[28] The initial oxidation and reduction processes of complexes $[\mathbf{1}]^{+}$ and $[\mathbf{2}]^{+}$ are electrochemically reversible on the time scale of the experiment. Compared to $[Ru(tpy)_2]^{2+}$ both the anodic and cathodic process of $[\mathbf{1a}]^{+}$ are negatively shifted as a result of the strong σ-donor carbon atom. The initial oxidation process is stronger affected with a shift of 1.07 V compared to a shift of 0.37 V for the reduction process. Additionally, an irreversible second oxidation process is observed at $E_{p,a} = 0.66$ V. The extent of the negative shift of the initial oxidation electrode potential compared to $[Ru(tpy)_2]^{2+}$ is with 0.77 V smaller in $[\mathbf{2a}]^{+}$ than in $[\mathbf{1a}]^{+}$. Also the reduction potential of $[\mathbf{2a}]^{+}$ is less affected. Similar to $[\mathbf{1a}]^{+}$ an irreversible second oxidation process is observed, but at increased potential with $E_{p,a} = 1.26$ V. The chloride substituent in both $[\mathbf{1b}]^{+}$ and $[\mathbf{2b}]^{+}$ results in a positive shift of the oxidation and reduction electrode potentials, in line with the electron-accepting nature of this moiety. The slightly less electronegative bromine atom exerts a slightly smaller change than is observed for the chloride.

Electronic Absorption Spectroscopy. The solution UV−vis spectra of the ruthenium(II) complexes $[\mathbf{1}]^{+}$ and $[\mathbf{2}]^{+}$ as well as of ruthenium(III) complexes $[\mathbf{1}]^{2+}$ and $[\mathbf{2}]^{2+}$ are summarized in Table 3. Ruthenium complex $[\mathbf{1a}]^{2+}$ was generated *in situ* by addition of $CuCl_2$ to the aqueous solution of the ruthenium(II) precursor following literature procedures.[20,21] Similarly, $[\mathbf{1b}]^{2+}$ and $[\mathbf{1c}]^{2+}$ were also prepared *in situ*. After reduction with either $Na_2S_2O_3$ or iPr$_2$NH, the original absorption spectra of the ruthenium(II) complexes were completely recovered. Ruthenium(III) complexes $[\mathbf{2}]^{2+}$ in MeCN solution were generated via chemical oxidation using $[Ce(NO_3)_6](NH_4)_2$, and the spectra of the corresponding ruthenium(II) complexes were completely recovered upon addition of a chemical reductant. Spectra obtained for the bromide substituted complexes $[\mathbf{1c}]^{n+}$ and $[\mathbf{2c}]^{n+}$ are essentially identical to those obtained for the chloride substituted complexes $[\mathbf{1b}]^{n+}$ and $[\mathbf{2b}]^{n+}$, respectively.

Additionally we investigated the nature of the lowest energy transitions of the ruthenium(II) and ruthenium(III) complexes $[\mathbf{1a}]^{n+}$, $[\mathbf{1b}]^{n+}$, $[\mathbf{2a}]^{n+}$, and $[\mathbf{2b}]^{n+}$ using the time-dependent density functional theory (TD-DFT) approach. Calculations were performed at the DZ Dunning[29,30] level of theory with the Stuttgart RSC 1997 ECP relativistic core potential[31] for ruthenium using the B3LYP functional. TD-DFT calculations were run on optimized geometries at the same level of theory. A complete listing of electronic transitions, energy levels, and isovalue plots[32] of the frontier molecular orbitals can be found in the Supporting Information. Selected plots of $[\mathbf{1a}]^{+}$ and $[\mathbf{1a}]^{2+}$ are displayed in Figure 3. In addition to isovalue plots we have used an extended Mulliken population analysis[33] in the spatial assignment of the individual orbitals, Table 4 and Figure 4.

Generally, in polypyridine complexes of ruthenium(II), the strong absorptions in the UV are assigned to ligand based $\pi-\pi^*$ transitions (IL), and absorptions in the visible part of the spectrum as metal-to-ligand charge transfer transitions (MLCT).[27,28] Transitions are consistently predicted by TD-DFT at increased energy but reproduce the spectra, and replicate their changes upon halogenation. The nature of the low energy visible transitions for the cyclometalated $[\mathbf{1}]^{+}$ and $[\mathbf{2}]^{+}$ are also mainly MLCT, with the tpy ligand as acceptor state and originating from different metal levels. A more elaborate analysis of the electronic and optical properties of a series of cyclometalated complexes, including $[\mathbf{2}]^{+}$ is published elsewhere.[24]

The absorption spectra of the ruthenium(III) complexes are highly sensitive toward substitution. For instance, a clear peak

(27) Maestri, M.; Armaroli, N.; Balzani, V.; Constable, E. C.; Thompson, A. M. W. C. *Inorg. Chem.* **1995**, *34* (10), 2759–2767.
(28) Juris, A.; Balzani, V.; Barigelletti, F.; Campagna, S.; Belser, P.; Von Zelewsky, A. *Coord. Chem. Rev.* **1988**, *84*, 85–277.
(29) Dunning, T. H., Jr. *J. Chem. Phys.* **1970**, *53* (7), 2823–33.
(30) Dunning, T. H., Jr.; Hay, P. J. *Mod. Theor. Chem.* **1977**, *3* (Methods Electron. Struct. Theory), 1–27.
(31) Andrae, D.; Haussermann, U.; Dolg, M.; Stoll, H.; Preuss, H. *Theor. Chim. Acta.* **1990**, *77* (2), 123–141.
(32) Schaftenaar, G.; Noordik, J. H. *J. Comput. Aided Mater. Des.* **2000**, *14* (2), 123–134.
(33) Mulliken, R. S. *J. Chem. Phys.* **1955**, *23*, 1833–40.

Table 3. Electronic Absorption Spectroscopy Data of Complexes $[\mathbf{1}]^{n+}$ in H_2O Solution and $[\mathbf{2}]^{n+}$, $[\mathbf{3}]^{2n+}$,[20] and $[Ru(tpy)_2]^{2+}$ in MeCN Solution

	λ_{max} (nm) (ε (10^3 M^{-1} cm^{-1})[a])	
complex	$n = 1$	$n = 2$
$[\mathbf{1a}]^{n+}$	622 (5.4), 586 (5.5), 518 (5.5), 384 (6.1), 323 (30.9), 280 (25.0)	540 (sh), 470 (3.8), 380 (3.3)
$[\mathbf{1b}]^{n+}$	620 (sh), 582 (5.6), 515 (5.3), 368 (6.7), 323 (29.6), 279 (21.0)	571 (5.2), 457 (3.3), 373 (3.5)
$[\mathbf{1c}]^{n+}$	620 (sh), 582 (5.6), 515 (5.3), 366 (6.8), 323 (30.6), 279 (20.8)	576 (5.4), 485 (3.0), 373 (3.1)
$[\mathbf{2a}]^{n+}$	499 (14.4), 424 (9.6), 368 (sh), 316 (37.0), 277 (47.0), 243 (49.8)	740 (sh), 629 (2.0), 390 (9.7), 328 (24.5)
$[\mathbf{2b}]^{n+}$	508 (13.2), 421 (7.8), 370 (7.7), 315 (35.6), 275 (50.2), 240 (45.3)	677 (2.7), 402 (8.8), 328 (21.9), 273 (45.3)
$[\mathbf{2c}]^{n+}$	507 (13.2), 421)7.5), 371 (7.2), 315 (35.2), 275 (51.4), 240 (44.2)	676 (2.7), 403 (8.6), 328 (21.7), 280 (43.0)
$[\mathbf{3}]^{2n+}$	618 (15.8), 593 (16.7), 528 (18.1), 377 (37.2), 324 (73.0), 280 (59.5)	657 (117.0), 306 (38.4), 275 (46.6), 201 (170.3)
$[Ru(tpy)_2]^{2+}$	475 (14.7), 308 (63.4), 270 (38.8), 225 (sh)	

[a] sh = shoulder.

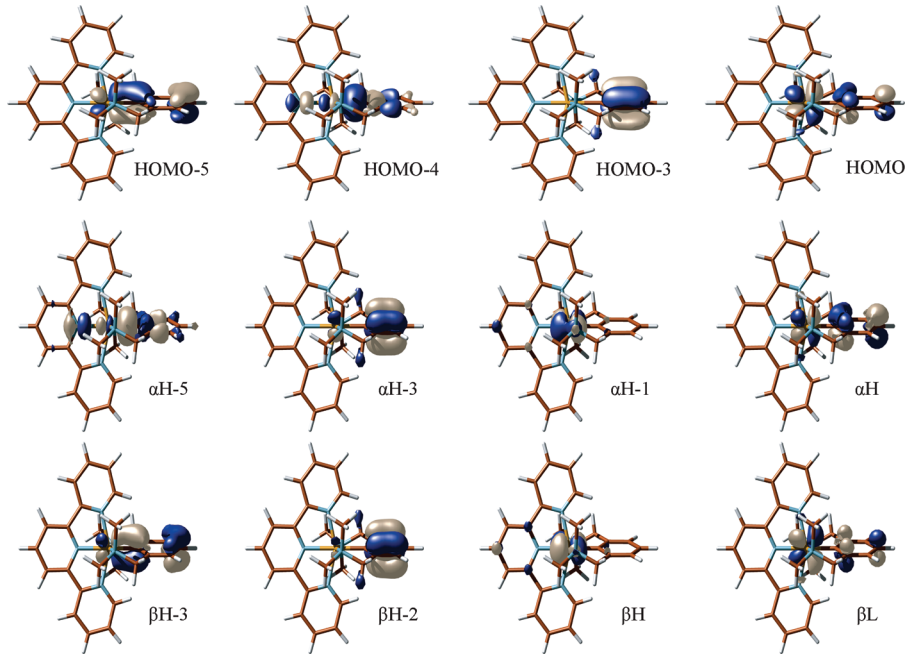

Figure 3. Isovalue (value = 0.05) plots of selected frontier orbitals of $[\mathbf{1a}]^{+}$ (top) and $[\mathbf{1a}]^{2+}$ (middle and bottom).

Table 4. Mulliken Population (Electron) on Ru of the Frontier Orbitals in $[Ru(tpy)_2]^{2+}$[24] and Complexes $[\mathbf{1a}]^{n+}$ and $[\mathbf{1b}]^{n+}$[a]

			$[\mathbf{1a}]^{2+}$		$[\mathbf{1b}]^{2+}$	
$[Ru(tpy)_2]^{2+}$	$[\mathbf{1a}]^{+}$	$[\mathbf{1b}]^{+}$	α	β	α	β
0.00	0.01	0.01	0.10	0.04	0.02	0.17
0.71	0.78	0.78	0.63	0.74	0.71	0.77
0.71	0.66	0.67	0.70	0.73	0.70	0.72
0.68	0.56	0.53	0.29	0.62	0.21	0.59
0.08	0.15	0.15	0.05	0.06	0.05	0.06

[a] Mulliken population sums to one electron per molecular orbital and spin orbital. Double lines indicate the border between occupied and unoccupied levels.

is observed at 571 nm for $[\mathbf{1b}]^{2+}$, whereas no such clear feature is present in the visible region for $[\mathbf{1a}]^{2+}$. Apart from several weak excitations, a single strong transition is present in the energy envelope of predicted excitations for both $[\mathbf{1a}]^{2+}$ and $[\mathbf{1b}]^{2+}$. This transition is of NCN-pincer-to-metal charge transfer character. Destabilization of the donor-orbital of this transition by interaction with the chloride in $[\mathbf{1b}]^{2+}$ is responsible for red shifting the predicted transition by almost 2000 cm^{-1}. A more detailed analysis of the electronic absorption spectra can be found as Supporting Information.

Discussion

In the 1980s we reported the oxidation of NCN-pincer d^8-platinum complexes such as [PtCl(NCN)] with copper(II) halide salts to yield the corresponding, stable d^6-platinum(IV) compounds (i.e. $[PtCl_3(NCN)]$).[34,35] The same reaction afforded in the case of the [NiCl(NCN)] compounds the surprisingly stable d^7-nickel(III) complexes,[36−39] which was the first air-stable true nickel(III) compound. EPR showed that the unpaired electron is located in the metal d_{z^2} orbital, enabling the compound to act as a persistent radical. These characteristics could be exploited by using [NiBr(NCN)] as catalyst in, for instance atom

(34) van Koten, G.; van Beek, J. A. M.; Wehman-Ooyevaar, I. C. M.; Muller, F.; Stam, C. H.; Terheijden, J. *Organometallics* **1990**, *9* (4), 903–12.
(35) van Beek, J. A. M.; van Koten, G.; Smeets, W. J. J.; Spek, A. L. *J. Am. Chem. Soc.* **1986**, *108* (16), 5010–11.

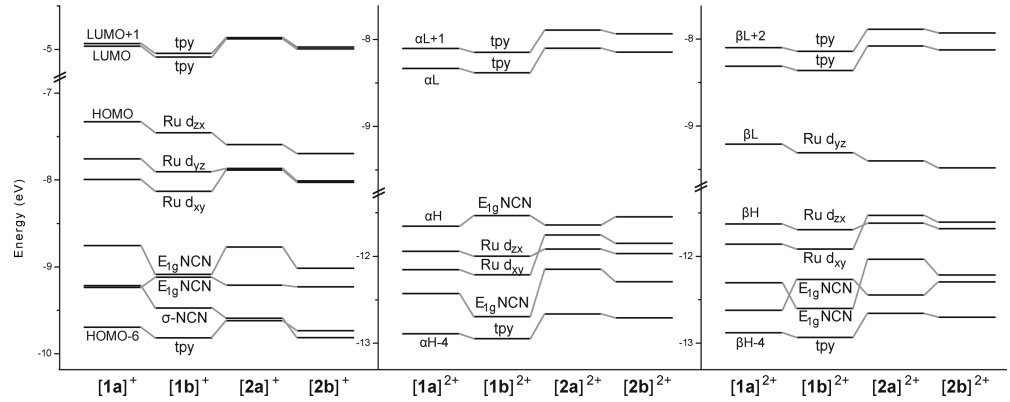

Figure 4. Energies and assignment of the 7 HOMOs and 2 LUMOs for $[\mathbf{1a}]^+$, $[\mathbf{1b}]^+$, $[\mathbf{2a}]^+$, and $[\mathbf{2b}]^+$ (left), the 5 alpha HOSOs and 2 alpha LUSOs (middle) and 5 beta HOSOs and 3 beta LUSOs (right) for $[\mathbf{1a}]^{2+}$, $[\mathbf{1b}]^{2+}$, $[\mathbf{2a}]^{2+}$, and $[\mathbf{2b}]^{2+}$. Orbitals of similar origin are connected via gray lines.

transfer radical addition (ATRA) reactions such as the Kharasch addition, and as catalyst in living polymerization by atom transfer polymerization (ATRAP).[40] The NCN-pincer proved beneficial in these cases as it stabilized the higher oxidation states while it is relatively inert itself.

Also in the case of the ruthenium(II) complexes, the strong σ-donor characteristics of the NCN-pincer ligand result in negatively shifted oxidation potentials, and the ruthenium(II) complexes could therefore easily be oxidized to a higher oxidation state using copper(II) salts.[20] However, one-electron oxidation of the d^6-ruthenium(II) complex [Ru(NCN)(tpy)]$^+$ ($[\mathbf{1a}]^+$) with $CuCl_2$ in methanol solution did not stop at the stage of the corresponding d^5-ruthenium(III) species, but resulted in the formation of a mixture of ruthenium(III) products resulting from dimerization (C−C coupling, 90%) ([{Ru(tpy)}$_2$(μ-NCN-NCN)](CuCl$_2$)$_4$, $[\mathbf{3}]^{4+}$) and halogenation (C−X coupling, < 10%) ([Ru(4-Cl-NCN)(tpy)]$^+$, $[\mathbf{1b}]^+$) reactions.[20,21] Interestingly, the phosphor coordinated PCP-pincer [Ru(PCP)(tpy)]$^+$ (PCP = 2,6-bis(diphenylphosphinomethyl)phenyl) complex also undergoes dimerization upon oxidation with $CuCl_2$ in methanol solution, albeit with only 15% yield in the dimer and with formation of 40% of the *para*-chlorinated complex [Ru(4-Cl-PCP)(tpy)]$^+$.[22] In a similar fashion, the dimer [{Ru(ttpy)}$_2$(μ-N^C^N−N^C^N)]$^{2+}$ was found during the preparation of [Ru(N^C^N)-(ttpy)](PF$_6$) when a large excess of $AgBF_4$ was used.[25,26]

Thus, whereas the ruthenium(II) complexes $[\mathbf{1a}]^+$ and $[\mathbf{2a}]^+$ are stable, both as solid and in solution, the corresponding ruthenium(III) complexes indeed display rich and interesting chemistry. To investigate this difference, we will first discuss the electronic configuration of the ruthenium(II) complexes and the changes that are induced upon one-electron oxidation, using the electrochemical and photophysical data as well as results from the DFT calculations. Subsequently, we will discuss the reaction mechanism, which allows differentiation between halogenation and dimerization. This mechanism is supported by kinetic data obtained by following both the halogenation and dimerization reactions with electronic absorption spectroscopy.

For ease of discussion we to use localized descriptions, but one need to keep in mind that significant interaction between the metal and the ligands is present. Like noncyclometalated polypyridine ruthenium(II) complexes, the initial oxidation processes of $[\mathbf{1}]^+$ and $[\mathbf{2}]^+$ are indeed metal-based. The HOMOs of the ruthenium(II) complexes are predominantly metal-based and the lowest unoccupied spin orbitals (LUSOs), βL, of the resulting ruthenium(III) complexes are largely associated with the d_{yz} orbital of the metal center (figure 3). The large negative shift (1.07 V) of the electrode potential for the first oxidation compared to $[Ru(tpy)_2]^{2+}$ ($E_{1/2}$ = 0.89 V) is a result of the electron rich metal center due to the strong σ-donation from the anionic carbon center, caused by the interaction between the σ-donating carbon and the unoccupied d_{z^2} ruthenium orbital, which possesses the correct symmetry.

In the ruthenium(III) complex $[\mathbf{1a}]^{2+}$, the electron distribution is reordered and the highest occupied alpha spin orbital (αH) is associated with the cyclometalated ligand, possessing only 29% population on the metal center. Consequently, the second oxidation process of $[\mathbf{1a}]^+$ is assigned to oxidation of the NCN-pincer, which is in line with the irreversible nature of this oxidation process. Interestingly, this implies that although the initial oxidation is metal-based, the unpaired electron in the resulting d^5-ruthenium(III) complexes is localized, at least to some extent, on the cyclometalated ligand. In contrast, the unpaired electron in the d^7 square-pyramidal nickel(III) complex [NiCl$_2$(NCN)] and the isoelectronic cobalt(II) complex [Co-Cl(NCN)(pyridine)] is associated with the metals' d_{z^2}, orbital as indicated by EPR spectroscopy.[36−38,41] The NCN-pincers' π-system cannot directly interact with this metal based unpaired electron and no chemistry connected to the cyclometalated ligand was observed in that case. The strong involvement of the NCN-pincer in the highest occupied spin orbitals (HOSOs) in $[\mathbf{1a}]^{2+}$ is also reflected by the red-shift of almost 2000 cm^{-1} of main visible transition of $[\mathbf{1}]^{2+}$ upon chlorination.

The most noteworthy effect of the chloride in $[\mathbf{1b}]^+$ compared to the hydrogen in $[\mathbf{1a}]^+$ is the interaction of the chloride with the aryl based E_{1g} HOMO-3 and HOMO-5, Figure 3. Whereas the HOMO-3 does not interact directly either with the chlorine or the metal center since they are in its nodal plane, the stabilization of the HOMO-5 by interaction with the metal center

(36) Grove, D. M.; van Koten, G.; Zoet, R.; Murrall, N. W.; Welch, A. J. *J. Am. Chem. Soc.* **1983**, *105* (5), 1379–80.
(37) Grove, D. M.; van Koten, G.; Mul, P.; Van der Zeijden, A. A. H.; Terheijden, J.; Zoutberg, M. C.; Stam, C. H. *Organometallics* **1986**, *5* (2), 322–6.
(38) Grove, D. M.; van Koten, G.; Mul, P.; Zoet, R.; Van der Linden, J. G. M.; Legters, J.; Schmitz, J. E. J.; Murrall, N. W.; Welch, A. J. *Inorg. Chem.* **1988**, *27* (14), 2466–73.
(39) van de Kuil, L. A.; Grove, D. M.; Gossage, R. A.; Zwikker, J. W.; Jenneskens, L. W.; Drenth, W.; van Koten, G. *Organometallics* **1997**, *16* (23), 4985–4994.
(40) Gossage, R. A.; van de Kuil, L. A.; van Koten, G. *Acc. Chem. Res.* **1998**, *31* (7), 423–431.
(41) Van der Zeijden, A. A. H.; van Koten, G. *Inorg. Chem.* **1986**, *25* (26), 4723–5.

Scheme 2. Resonance Structures for $[\mathbf{1a}]^{2+}$

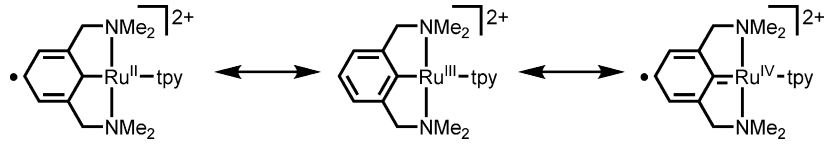

is counteracted by destabilization due to interaction with the chloride. The energetic difference between the two E_{1g} NCN-pincer based occupied orbitals is thus significantly reduced. This effect is somewhat stronger in the oxidized complexes, reversing the energetic order of the levels between $[\mathbf{1a}]^{2+}$ and $[\mathbf{1b}]^{2+}$, Figure 4.

It is well-known that the electronic properties of a NCN pincer metal center can be tuned by careful selection of the *para*-substituent. For instance, in a series of NCN-pincer platinum complexes, a clear correlation was observed between the Hammett parameter of the *para*-substituent and the ^{195}Pt chemical shift of the metal center.[42,43] The same holds for the NCN-pincer nickel(II) complexes which show correlation between their Ni^{II}/Ni^{III} oxidation potentials and the substituents' Hammett parameter. It is this very interaction via the NCN pincers' orbitals that is responsible for tuning the electronic characteristics of the metal center upon *para*-substitution. In the current ruthenium complexes, this interaction is reflected by the positive shift of the oxidation potential of $[\mathbf{1b}]^{+}$ compared to $[\mathbf{1a}]^{+}$, as is also predicted by stabilization of the upper HOMOs.

Of significant importance to the reactivity of $[\mathbf{1a}]^{2+}$ is the fact that the HOSO (αH) is thus best described as associated with the cyclometalated ligand albeit with a significant component on the metal center. The unpaired electron in $[\mathbf{1a}]^{2+}$ is at least partly localized on the cyclometalated aryl moiety, resulting in quinone type resonance structures, Scheme 2. The 2,3:5,6-hexadieen moiety can be formed either by formal electron transfer from the aryl ring to the ruthenium center (comparable to what is observed for the d^{10}-platinum $[Pt(PCP)]^{-}$ complex[44]) or by formation of a carbon-to-ruthenium double bond, thereby formally oxidizing the ruthenium center (as proposed for the $[\mathbf{3}]^{4+}$ dimer[20,21]). The first resonance structure seems more likely to contribute significantly as it is supported by the fact that oxidation is associated with a decrease in Mulliken population of only 0.13 electron on the ruthenium center. These resonance structures are corroborated by bond length alternation in the aryl moiety, with the $C_{ortho}-C_{meta}$ bond being the shortest in the calculated structures. Unfortunately, due to the standard uncertainties of the atomic coordinates and the thermal motion of the atoms, X-ray crystal structure determination is not a suitable method to detect these minor changes in bond lengths alternations (Table 1). With the unpaired electron partly localized on the *para* position, reactions associated with radical mechanisms can be anticipated. The same reasoning can be applied for $[\mathbf{2a}]^{2+}$, in which the radical character is expected to be slightly dissipated by delocalization over the pendant pyridine rings of the N^C^N ligand.

***Para*-Halogenation vs Dimerization of Ruthenium(III) Complexes.** The d^6-ruthenium(II) complex $[\mathbf{1a}]^{+}$ is chemically stable in solution, but due to the specific properties of the ruthenium(III) complexes dimerization and halogenation is observed for $[\mathbf{1a}]^{2+}$. The formation of $[\mathbf{1b}]^{+}$ as a side product with <10% yield in the dimerization of $[\mathbf{1a}]^{+}$ using three equivalents of $CuCl_2$ is significant in view of a possible reaction mechanism. After oxidation of $[\mathbf{1a}]^{+}$ to $[\mathbf{1a}]^{2+}$ in MeOH solution, which is almost instantaneous and fully reversible, the competitive reaction with the excess persistent radical[45] $CuCl_2$ results in irreversible formation of $[\mathbf{1b}]^{+}$. Indeed, when a large excess of $CuCl_2$ was used $[\mathbf{1b}]^{2+}$ could be selectively prepared in good yield after overnight stirring at room temperature. The reported dimerization of $[Ru(N^C^N)(ttpy)]^{+}$ was devoid of such side products as no other potential reaction partners were present in solution.

The electronic absorption spectra of the ruthenium(III) complexes $[\mathbf{1a}]^{2+}$ and $[\mathbf{1b}]^{2+}$ differ significantly, and the progress of the reaction could be monitored by UV−vis spectroscopy, Figure 5. Using a large excess of $CuCl_2$ (0.65 M) compared to $[\mathbf{1a}]^{+}$ (1.1 mM) selective formation of $[\mathbf{1b}]^{2+}$ is expected. The time dependent concentration of $[\mathbf{1a}]^{2+}$ as derived from the absorption at 571 nm, plotted as first-order kinetics is also shown in Figure 5, and the reaction accurately obeys first order kinetics as expected, with rate constant $k = 2 \times 10^{-4}$ s^{-1}. From this it is also evident that $[\mathbf{1a}]^{2+}$ reacts with the excess of $CuCl_2$ under an one-electron chloride transfer, and not with $CuCl_2^{-}$ formed in the oxidation step. Unfortunately, these measurements could only be performed at room temperature in the current setup, yielding no further kinetic information.

When only a small excess of $CuCl_2$ is used (32 mM) compared to $[\mathbf{1a}]^{+}$ (6.2 mM), the formation of $[\mathbf{3}]^{4+}$ can be

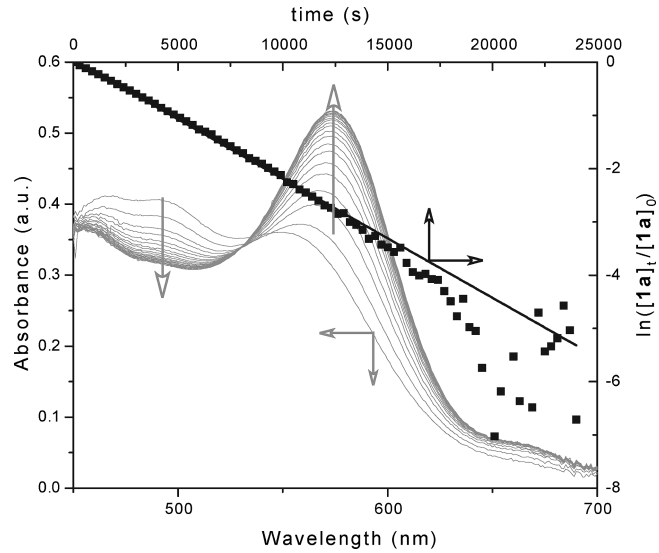

Figure 5. Spectral changes during reaction of $[\mathbf{1a}]^{2+}$ in the presence of a large excess $CuCl_2$ (gray, left and bottom axes) and $\ln([\mathbf{1a}]^{2+}_t/[\mathbf{1a}]^{2+}_0)$ as a function of time (black squares, right and top axes, line is fitted through first 90% conversion).

(42) Slagt, M. Q.; Rodriguez, G.; Grutters, M. M. P.; Klein Gebbink, R. J. M.; Klopper, W.; Jenneskens, L. W.; Lutz, M.; Spek, A. L.; van Koten, G. *Chem.—Eur. J.* **2004**, *10* (6), 1331–1344.
(43) Batema, G. D.; Lutz, M.; Spek, A. L.; van Walree, C. A.; Donegá, C. d. M.; Meijerink, A.; Havenith, R. W. A.; Pérez-Moreno, J.; Clays, K.; Büchel, M.; Dijken, A. v.; Bryce, D. L.; van Klink, G. P. M.; van Koten, G. *Organometallics* **2008**, *27* (8), 1690–1701.
(44) Schwartsburd, L.; Cohen, R.; Konstantinovski, L.; Milstein, D. *Angew. Chem., Int. Ed.* **2008**, *47* (19), 3603–3606.

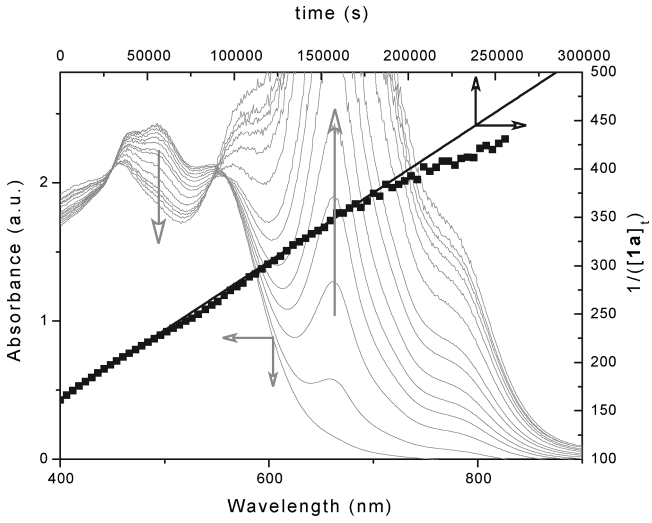

Figure 6. Spectral changes during reaction of $[\mathbf{1a}]^{2+}$ in the presence of 5 equiv of $CuCl_2$ (gray, left and bottom axes) and $1/([\mathbf{1a}]^{2+}{}_t)$ as a function of time (black squares, right and top axes, line is fitted through first 50% conversion).

Scheme 3. Proposed Mechanisms of Reactions of $[\mathbf{1a}]^{+}$ with $CuCl_2$

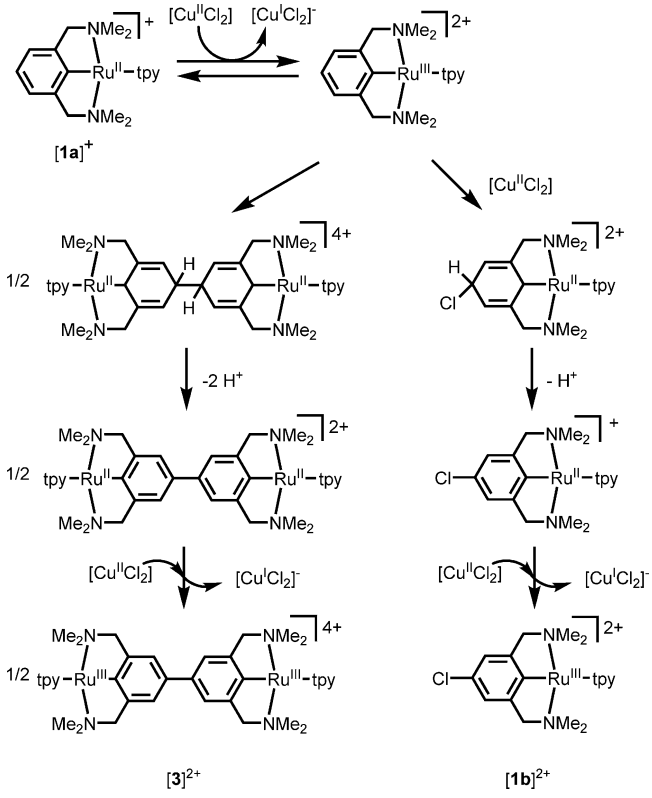

observed at 657 nm, Figure 6. After formation, $[\mathbf{1a}]^{2+}$ slowly dimerizes to the initially formed $[\mathbf{3}]^{2+}$, which is subsequently quickly oxidized to form $[\mathbf{3}]^{4+}$, consuming another equivalent of $CuCl_2$. Since a concentrated solution was needed to obtain reasonable reaction rates, the rise in absorption at 750 nm associated with the formation of $[\mathbf{3}]^{4+}$ was used, rather than at the absorption maximum. This bimolecular C−C coupling reaction obeys second order kinetics with rate constant $k = 1 \times 10^{-3}\ M^{-1}\ s^{-1}$, Figure 6.

In the proposed reaction mechanism, Scheme 3, it is the persistent nature of the organometallic radical that plays a crucial role in the organic chemistry on the aryl ring which is σ-bonded to the metal center. In fact it is the electronic configuration of the metal center that triggers the chemistry on the organic part and at the same time controls the reactive odd electron organic intermediates, *vide supra*. Rather than acting as a persistent catalyst which controls the formation and protection of the external reacting radical and the product radical, as in the ATRA and ATRAP reactions,[40] the metal in the present case controls an intramolecular radical event.

It is interesting to note that the dimerization reactions of $[\mathbf{1a}]^{+}$ and [Ru(N^C^N)(ttpy) seem very similar to the dimerization of triarylamines via formation of the radical cation by chemical oxidation with $Cu(ClO_4)_2$, recently reported by Gopidas et al.[46] Using results from EPR, spectroscopic and kinetic studies the authors proposed a mechanism in which the radical cation of the triarylamine reacts with a second radical cation. After elimination of two protons the dimeric compound was obtained selectively, and directly oxidized by the excess oxidant in solution. It seems likely that the dimerization of $[\mathbf{1a}]^{2+}$ to $[\mathbf{3}]^{4+}$ follows a similar mechanism, Scheme 3. Alternatively, the reaction of $[\mathbf{1a}]^{2+}$ with a second equivalent of the persistent radical $CuCl_2$ instead of a second equivalent of $[\mathbf{1a}]^{2+}$ forms the corresponding halogenated intermediate, which indeed obeys the expected first order kinetics. After elimination of a proton and subsequent oxidation by an additional equivalent of $CuCl_2$ the product $[\mathbf{1b}]^{2+}$ is formed. The radical nature of the complex can be used to explain other observations as well, such as the observation of brominated side product in the reaction of PCP-iridium species,[19] and that it is important to realize that cyclometalated ligands are not always innocent ligands.

We have noted previously that when the metal moiety is qualitatively seen as a rather elaborate substituent on the aryl ring, it possesses comparable electronic properties (i.e., similar Hammett[47] σ_p parameter and *ortho*- and *para*-directing and activating influence for electrophilic substitution reactions) as a NMe_2 group.[1,43,48] (It is this observation that has led us to develop organometallic stilbenoid non linear optics materials as analogues of the well-known 4-dimethylamino-4′-nitrostilbene (DANS) molecule. This similarity can now be further extended to the oxidized species as well in which the organometallic moiety in $[\mathbf{1a}]^{2+}$ influences the reactivity of the aryl ring in way comparable to that of the R_2N^{+} moiety.)

As also $[Ru(N^C^N)(ttpy)]^{+}$ is known to form C−C coupled dimeric species upon oxidation, the very similar complex $[\mathbf{2a}]^{+}$ was expected to undergo halogenation with copper(II) salts. However, upon addition of $[\mathbf{2a}]^{+}$ to a solution of $CuCl_2$ in MeOH no color change was observed, and chlorination occurred selectively but sluggish. On the other hand, addition of $[\mathbf{2a}]^{+}$ to a solution of $CuBr_2$ in MeOH resulted in a color change from red to green and complete conversion to $[\mathbf{2c}]^{2+}$ was achieved at room temperature overnight, that is, on the same time scale as for $[\mathbf{1c}]^{2+}$. It seems unlikely that the difference in reaction rate originates from a significant difference in the speed between chlorination and bromination reactions on complex $[\mathbf{2a}]^{2+}$, which was not observed for $[\mathbf{1a}]^{2+}$. A more likely reason is incomplete oxidation by $CuCl_2$, as indicated by the retention of the typical red color of $[\mathbf{2a}]^{+}$. The equilibrium between $[\mathbf{2a}]^{+}$ and $[\mathbf{2a}]^{2+}$,

(45) Fischer, H. *Chem. Rev.* **2001**, *101* (12), 3581–3610.
(46) Sreenath, K.; Suneesh, C. V.; RatheeshKumar, V. K.; Gopidas, K. R. *J. Org. Chem.* **2008**, *73* (8), 3245–3251.
(47) Hansch, C.; Leo, A.; Taft, R. W. *Chem. Rev.* **1991**, *91* (2), 165–195.
(48) Batema, G. D.; van de Westelaken, K. T. L.; Guerra, J.; Lutz, M.; Spek, A. L.; van Walree, C. A.; Donega, C. D.; Meijerink, A.; van Klink, G. P. M.; van Koten, G. *Eur. J. Inorg. Chem.* **2007**, (10), 1422–1435.

which lies at the side of $[\mathbf{2a}]^+$, is fast as almost instantaneous oxidation is observed using $CuBr_2$ or $[Ce(NO_3)_6](NH_4)_2$. Partial oxidation will result in a low concentration of ruthenium(III) $[\mathbf{2a}]^{2+}$, decreasing the speed of chlorination since the rate of this reaction is first order in $[\mathbf{2a}]^{2+}$. Heating the reaction mixture under reflux increased the overall rate of chlorination. It can be reasoned that the higher temperature increases the rate of the chlorination step, but it is also possible that the position of the equilibrium between $[\mathbf{2a}]^+$ and $[\mathbf{2a}]^{2+}$ is shifted to side of $[\mathbf{2a}]^{2+}$. The positively shifted oxidation potential of $CuBr_2$ compared to $CuCl_2$ resulted in complete oxidation of $[\mathbf{2a}]^+$ to $[\mathbf{2a}]^{2+}$ and hence to an overall reaction rate similar to that observed for halogenation of $[\mathbf{1a}]^{2+}$.

Bromination reactions on cyclometalated complexes of ruthenium as well as other metals have been performed before,[1] using for instance NBS[15,16] or pyridinium tribromide.[13,17,18] Although these reagents are indeed rather gentle compared to the conditions used for halogenation of the uncoordinated ligands, they resulted in complete decomposition of $[\mathbf{1a}]^+$. Bromination using $CuBr_2$ as described here is very mild and no decomposition of $[\mathbf{1a}]^+$ or $[\mathbf{1c}]^+$ was observed. Halogenations using CuX_2 might thus lead to a larger functional group tolerance and expand the scope of functionalization of metal complexes.

Conclusions

A new method for very mild, selective halogenation of cycloruthenated complexes using oxidation with CuX_2 in MeOH solution is described. Upon chemical oxidation of the NCN-pincer ruthenium(II) complex $[\mathbf{1a}]^+$ in MeOH solution, the ruthenium(III) complex $[\mathbf{1a}]^{2+}$ is formed and present as a persistent radical cation. In this ruthenium(III) species, the unpaired electron is at least partially localized on the cyclometalated ligand as deduced from experimental results and corroborated by DFT calculations, but protected by interaction with the metal center. Homocoupling reaction of this organometallic radical results in the previously reported formation of the dimeric complex $[\mathbf{3}]^{4+}$,[20] obeying second order kinetics in $[\mathbf{1a}]^{2+}$. When an excess of CuX_2 is present, competitive reaction of $[\mathbf{1a}]^{2+}$ with the radical species CuX_2 yields the halogen substituted complex, obeying the expected first order reaction kinetics. These results are in agreement with the proposed radical mechanism in which the ruthenium(III) species $[\mathbf{1a}]^{2+}$ undergoes coupling to a second radical present in solution. The difference in rate law between halogenation and dimerization allows excellent control over the product distribution. The N^C^N ruthenium(II) tpy complex $[\mathbf{2a}]^+$ can also be halogenated in this fashion, and the positively shifted oxidation potential of $[\mathbf{2a}]^+$ compared to $[\mathbf{1a}]^+$ results in partial oxidation by $CuCl_2$ causing a particularly well controllable reaction.

Experimental Section

General. All air-sensitive reactions were performed under a dry nitrogen atmosphere using standard Schlenk techniques. Absolute solvents were dried over appropriate drying agents and distilled before use. All other solvents and reagents were purchased and used as received. ^1H and $^{13}C\{^1H\}$ NMR spectra were recorded at 298 K on a Varian 400 MHz NMR system. NMR spectra were referenced to the solvent residual signal.[49] Spectral assignments were based on chemical shift and integral considerations as well as COSY and NOESY two-dimensional experiments. As a result of severe paramagnetic broadening of the resonances for the Ru^{3+} complexes integration of the ^1H NMR spectra was problematic and only selected carbon resonances could be observed. Solution UV−vis spectra were recorded on a Cary 50 Scan UV−visible spectrophotometer. Elemental analyses were carried out by Kolbe Mikroanalytisches Laboratorium (Mülheim an der Ruhr, Germany). MS measurements were carried out on an Applied Biosystems Voyager DE-STR MALDI-TOF MS. The compounds $[Ru(tpy)_2]^{2+}$,[50] $[\mathbf{1a}]^+$,[23] and $[\mathbf{2a}]^+$[24] were prepared following literature procedure.

Electrochemical Measurements. Cyclic voltammograms were recorded in a single compartment cell under a dry nitrogen atmosphere. The cell was equipped with a Pt microdisk working electrode, Pt wire auxiliary electrode and a Ag/AgCl wire reference electrode. The working electrode was polished with alumina nanopowder between scans. The potential control was achieved with a PAR Model 263A potentiostat. All redox potentials are reported against the ferrocene-ferrocenium (Fc/Fc^+) redox couple used as an internal or external standard.[51,52] All electrochemical samples were 10^{-1} M in $[n\text{-}Bu_4N]PF_6$ as supporting electrolyte in MeCN distilled over $KMnO_4$ and Na_2CO_3.

TD-DFT Calculations. DFT calculations were performed at the DZ Dunning[29,30] level of theory for carbon, nitrogen, chlorine and hydrogen, and using the Stuttgart RSC 1997 ECP relativistic core potential[31] for ruthenium using the B3LYP functional. Geometries were optimized using the Gamess UK[53] program package. Subsequent TD-DFT calculations were run on the optimized geometry at the same level of theory using the Gaussian[54] version 03 program package.

Kinetic Experiments. Solid $[\mathbf{1a}]^+$ was added to a MeOH solution of $CuCl_2$ of known concentration in a 1 mm path length QS cuvette, which resulted in an immediate color change from blue to red. The concentration of the resulting $[\mathbf{1a}]^{2+}$ was determined from the optical density of the solution. Spectra were obtained at regular intervals, and the normalized concentration of $[\mathbf{1a}]^{2+}$ was obtained using $C_{\mathbf{1a},t} = C_{\mathbf{1a},0} \times ((A_t - A_p)/(A_s - A_p))$, in which $C_{\mathbf{1a},t}$ and $C_{\mathbf{1a},0}$ are the concentration of $[\mathbf{1a}]^{2+}$ at time t and 0. The absorbance A_t, A_s, and A_p are at the detection wavelength at time t, time 0, and after full conversion, respectively.

Syntheses. [1a](Cl). ^1H NMR (400 MHz, CD_3CN): δ 8.70 (d, $^3J = 8.0$ Hz, 2H, A3,5), 8.54 (d, $^3J = 8.0$ Hz, 2H, B3), 8.18 (d, $^3J = 5.6$ Hz, 2H, B6), 8.01 (t, $^3J = 8.0$ Hz, 1H, A4), 7.93 (dd, $^3J = 8.0$ Hz, $^3J = 7.6$ Hz, 2H, B4), 7.45 (dd, $^3J = 7.6$ Hz, $^3J = 5.6$ Hz, 2H, B5), 7.25 (d, $^3J = 7.2$ Hz, 2H, D3,5), 7.03 (t, $^3J = 7.2$ Hz, 1H, D4), 3.64 (s, 4H, CH_2), 1.19 (s, 12H, CH_3). ^{13}C NMR (100 MHz, CD_3CN): δ 201.6, 161.4, 155.8, 153.6, 143.5, 135.3, 129.3, 127.8, 124.2, 122.7, 121.7, 121.1, 75.6, 52.1.

[1b](Cl). A solution of [**1a**](Cl) (292 mg, 0.52 mmol) in MeOH (10 mL) was slowly added dropwise to a solution of $CuCl_2$ (3.8 g, 22 mmol) in MeOH (25 mL). After addition was complete, the mixture was stirred at room temperature for 18 h.

(49) Gottlieb, H. E.; Kotlyar, V.; Nudelman, A. *J. Org. Chem.* **1997**, *62* (21), 7512–7515.
(50) Sullivan, B. P.; Calvert, J. M.; Meyer, T. J. *Inorg. Chem.* **1980**, *19* (5), 1404–7.
(51) Kolthoff, I. M.; Thomas, F. G. *J. Phys. Chem.* **1965**, *69* (9), 3049–58.
(52) Pavlishchuk, V. V.; Addison, A. W. *Inorg. Chim. Acta* **2000**, *298* (1), 97–102.
(53) Guest, M. F.; Bush, I. J.; van Dam, H. J. J.; Sherwood, P.; Thomas, J. M. H.; van Lenthe, J. H.; Havenith, R. W. A.; Kendrick, J. *Mol. Phys.* **2005**, *103* (6−8), 719–747.
(54) Frisch, M. J. et al. *Gaussian 03*; Gaussian, Inc: Wallingford, CT, 2004.

The solvent was removed *in vacuo* and the solid taken up in MeCN (4 mL), and subjected to column chromatography on silica (acetonitrile: H_2O: aq. 1 M $NaNO_3$ = 85:10:5). [**1b**]$(PF_6)_2$ was isolated from the red fractions by precipitation with aqueous KPF_6 and removal of acetonitrile *in vacuo*. Alternatively, [**1b**](Cl) was isolated after concentrating the fractions *in vacuo*, dissolving the solid in H_2O in the presence of an excess of $Na_2S_2O_3$ and NaCl and extraction of the dark blue solution with CH_2Cl_2. The organic phase was washed with brine and the solvent was removed *in vacuo*, yielding the product as a purple/blue solid (226 mg, 73%).

[1b](PF$_6$)$_2$. ^{1}H NMR (400 MHz, CD_3CN): δ 82.0 (s, 2H), 57.2 (s, 2H), 53.7 (s, 2H), 26.9 (s, 2H), 18.6 (s, 1H), 17.9 (s, 2H), 2.2 (s, 4H), 0.1 (s, 2H), −15.0 (s, 8H).

^{13}C NMR (100 MHz, CD_3CN): δ 179.5, 143.2, 141.2, 129.7, 128.8, 114.2, 100.2, 35.1, several resonances could not be resolved.

[1b](Cl). ^{1}H NMR (400 MHz, CD_3CN): δ 8.70 (d, ^3J = 8.0 Hz, 2H, A3,5), 8.55 (d, ^3J = 8.0 Hz, 2H, B3), 8.19 (d, ^3J = 5.2 Hz, 2H, B6), 8.02 (t, ^3J = 8.0 Hz, 1H, A4), 7.94 (dd, ^3J = 8.0 Hz, ^3J = 7.6 Hz, 2H, B4), 7.45 (dd, ^3J = 7.6 Hz, ^3J = 5.2 Hz, 2H, B5), 7.26 (s, 2H, D3,5), 3.63 (s, 4H, CH_2), 1.20 (s, 12H, CH_3).

^{13}C NMR (100 MHz, CD_3CN): δ 200.4, 161.2, 155.7, 153.7, 145.3, 135.6, 129.9, 127.9, 126.0, 124.2, 122.7, 121.0, 75.0, 52.1.

MALDI-TOF-MS (DHB Matrix): m/z = 560.11 [M$^+$] (calcd for $C_{27}H_{29}ClN_5Ru$, 560.12).

[1c](Cl). The same procedure was used as described for [**1b**](Cl). [**1a**](Cl) (498 mg, 0.89 mmol) was converted to [**1a**](Br) by anion exchange in H_2O prior to reaction. Using $CuBr_2$ (4.46 g, 20 mmol), the product was obtained as a purple/blue solid (400 mg, 70%) after ion exchange with brine.

[1c](PF$_6$)$_2$. ^{1}H NMR (400 MHz, CD_3CN): δ 83.2 (s, 2H), 57.7 (s, 2H), 53.7 (s, 2H), 26.9 (s, 2H), 18.6 (s, 1H), 17.9 (s, 2H), 2.1 (s, 4H), 0.2 (s, 2H), −15.0 (s, 6H).

Anal. calcd for $C_{27}H_{29}BrF_{12}N_5P_2Ru$: C, 36.25; H, 3.27; N, 7.83. Found: C, 36.50; H, 3.31; N, 8.01.

[1c](Cl). ^{1}H NMR (400 MHz, CD_3CN): δ 8.68 (d, ^3J = 8.0 Hz, 2H, A3,5), 8.52 (d, ^3J = 8.0 Hz, 2H, B3), 8.20 (d, ^3J = 8.0 Hz, 2H, B6), 8.02 (d, ^3J = 5.2 Hz, 2H, A4), 7.94 (dd, ^3J = 8.0 Hz, ^3J = 7.2 Hz, 2H, B4), 7.59 (dd, ^3J = 7.2 Hz, ^3J = 5.2 Hz, 2H, B5), 7.39 (s, 2H, D3,5), 3.66 (s, 4H, CH_2), 1.20 (s, 12H, CH_3).

^{13}C NMR (100 MHz, CD_3CN): δ 201.1, 161.2, 155.7, 153.8, 146.0, 135.6, 130.0, 127.9, 124.3, 123.6, 122.7, 113.7, 74.9, 52.1.

Anal. calcd for $C_{27}H_{29}BrN_5Ru(PF_6)$: C, 43.27; H, 3.90; N, 10.66. Found: C, 43.34; H, 3.97; N, 9.28.

MALDI-TOF-MS (DHB Matrix): m/z = 604.12 [M$^+$] (calcd for $C_{27}H_{29}BrN_5Ru$, 604.07).

[2b](PF$_6$). A mixture of [**2a**](PF_6) (29 mg, 0.042 mmol) and $CuCl_2$ (0.15 g, 0.87 mmol) in MeOH (25 mL) was heated under reflux for 72 h. After cooling down to room temperature, an excess of aqueous $Na_2S_2O_3$ and KPF_6 was added, and the mixture was stirred for 2 h. The suspension was filtered and the product extracted from the solids using MeCN (2 × 10 mL). The product was purified by column chromatography on SiO_2 (MeCN:H_2O:aq. 1 M $NaNO_3$ = 18:1:1), and obtained after anion exchange as a red solid (24 mg, 79%).

^{1}H NMR (400 MHz, CD_3CN): δ 8.76 (d, ^3J = 8.0 Hz, 2H, A3,5), 8.43 (d, ^3J = 8.0 Hz, 2H, B3), 8.29 (t, ^3J = 8.0 Hz, 1H, A4), 8.29 (s, 2H, D3,5), 8.17 (d, ^3J = 8.0 Hz, 2H, C3), 7.70 (dd,^3J = 8.0 Hz, ^3J = 7.6 Hz, 2H, B4), 7.64 (dd, ^3J = 8.0 Hz, ^3J = 7.6 Hz, 2H, C4), 7.08−7.13 (m, 4H, B6 + C6), 6.95 (dd, ^3J = 7.6 Hz, ^3J = 5.6 Hz, 2H, B5), 6.71 (dd, ^3J = 7.6 Hz, ^3J = 5.6 Hz, 2H, C5).

^{13}C NMR (100 MHz, CD_3CN): δ 219.9, 168.6, 160.0, 155.3, 153.9, 152.8, 144.4, 136.4, 136.1, 133.3, 127.3, 126.0, 124.4, 124.2, 123.3, 123.0, 121.0.

MALDI-TOF-MS (DHB Matrix): m/z = 600.13 [M$^+$] (calcd for $C_{31}H_{21}ClN_5Ru$, 600.05).

[2c](PF$_6$). [**2a**](PF_6) (68 mg, 0.095 mmol) was dissolved in CH_2Cl_2 (20 mL) and slowly added dropwise to a solution of $CuBr_2$ (0.39 g, 1.74 mmol) in MeOH (60 mL) and stirred at room temperature for 18 h. The solvent was removed *in vacuo* and the solid subjected to column chromatography on SiO_2 (MeCN:H_2O:1 M $NaNO_3$/H_2O = 18:1:1). The green fractions containing product were combined, and an excess of aqueous $Na_2S_2O_3$ and aqueous KPF_6 was added and the mixture was stirred at room temperature for 2 h during which the color turned deep red. After reducing the volume *in vacuo* the mixture was filtered and the product collected with MeCN and obtained as a red powder (68 mg, 91%).

^{1}H NMR (400 MHz, CD_3CN): δ 8.76 (d, ^3J = 8.0 Hz, 2H, A3,5), 8.43 (d, ^3J = 8.0 Hz, 2H, B3), 8.42 (s, 2H, D3,5), 8.30 (t, ^3J = 8.0 Hz, 1H, A4), 8.17 (d, ^3J = 8.0 Hz, 2H, C3), 7.70 (dd, ^3J = 8.0 Hz, ^3J = 8.0 Hz, 2H, B4), 7.64 (dd, ^3J = 8.0 Hz, ^3J = 8.0 Hz, 2H, C4), 7.08−7.12 (m, 4H, B6 + C6), 6.95 (dd, ^3J = 8.0 Hz, ^3J = 5.2 Hz, 2H, B5), 6.71 (dd, ^3J = 8.0 Hz, ^3J = 5.2 Hz, 2H, C5).

^{13}C NMR (100 MHz, CD_3CN): δ 220.5, 168.4, 159.9, 155.3, 153.8, 152.9, 144.9, 136.5, 136.1, 133.3, 127.2, 126.9, 124.4, 123.3, 123.0, 121.0, 113.2.

MALDI-TOF-MS (DHB Matrix): m/z = 644.06 [M$^+$] (calcd for $C_{31}H_{21}BrN_5Ru$, 644.00).

X-Ray Crystal Structure Determination of [1b](PF$_6$)$_2$. $[C_{27}H_{29}ClN_5Ru](PF_6)_2 \cdot CH_3CN$, Fw = 891.07, dark red plate, 0.45 × 0.28 × 0.05 mm^3, orthorhombic, $Fdd2$ (no. 43), a = 47.7085(2), b = 81.9437(4), c = 10.5045(18) Å, V = 41066.4(5) Å^3, Z = 48, D_x = 1.729 g/cm^3, μ = 0.728 mm^{-1}; 129442 Reflections were measured on a Nonius Kappa CCD diffractometer with rotating anode (graphite monochromator, λ = 0.71073 Å) up to a resolution of $(\sin\theta/\lambda)_{max}$ = 0.65 Å^{-1} at a temperature of 150 K. An absorption correction based on multiple measured reflections was applied[55] (0.88 − 0.96 correction range). 23323 Reflections were unique (R_{int} = 0.049). The structure was solved with Direct Methods (SHELXS-97[56]) and refined with SHELXL-97[56] against F^2 of all reflections. The structure contains a 3-fold pseudotranslational symmetry in the b-direction. Non-hydrogen atoms were refined freely with anisotropic displacement parameters. Hydrogen atoms were introduced in calculated positions and refined with a riding model. One PF_6 anion was refined with a disorder model. 1408 Parameters were refined with 46 restraints concerning the disordered PF_6 anion. $R1/wR2$ [$I > 2\sigma(I)$]: 0.0322/0.0676. $R1/wR2$ [all refl.]: 0.0422/0.0721. S = 1.034. Flack parameter[57] x = −0.034(11). Residual electron density between −0.66 and 0.76 e/Å^3. Geometry calculations and checking for higher symmetry was performed with the PLATON program.[58]

(55) Blessing, R. H. *J. Appl. Crystallogr.* **1997**, *30*, 421–426.
(56) Sheldrick, G. M. *Acta Crystallogr. A* **2008**, *64*, 112–122.
(57) Flack, H. D. *Acta Crystallogr. A* **1983**, *39* (6), 876–81.
(58) Spek, A. L. *J. Appl. Crystallogr.* **2003**, *36*, 7–13.

Acknowledgment. We gratefully acknowledge support from the European Commission through the funding of the project FULLSPECTRUM within the Sixth Framework Program under number SES6-CT-2003-502620. This work was partially supported (ML and ALS) by the Council for Chemical Sciences of The Netherlands Organization for Scientific Research (NWO/CW). The work of RWAH is part of the research programme of the Stichting voor Fundamenteel Onderzoek der Materie (FOM), which is financially supported by the NWO. We acknowledge NWO/NCF for supercomputer time on ASTER, SARA (The Netherlands, project number SG-032).

Supporting Information Available: Complete author listing for ref 54. Crystallographic cif files of [**1b**]$(PF_6)_2$. Detailed analysis of the electronic and photophysical properties of [**1a**]$^{n+}$, [**1b**]$^{n+}$, [**2a**]$^{n+}$, and [**2b**]$^{n+}$, as well as optimized molecular geometries, energies, Mulliken populations, and isodensity plots of the frontier molecular orbitals. This material is available free of charge via the Internet at http://pubs.acs.org.

JA9073276